A Mathematical Model for the Heterogeneity of Myocardial Perfusion Using Nitrogen-13-Ammonia

Klaas R. Visser, Joan G. Meeder, Johannes H.G.M. van Beek, Ernst E. van der Wall, Antoon T.M. Willemsen and Paul K. Blanksma

Department of Cardiology and PET Center, University Hospital Groningen, Groningen; Laboratory for Physiology, Institute for Cardiovascular Research, Free University, Amsterdam; and Department of Cardiology, Leiden University Hospital, Leiden, The Netherlands

Heterogeneity of left ventricular myocardial perfusion is an important clinical characteristic. Different aspects of this heterogeneity were analyzed. **Methods:** The coefficient of variation (v), characterizing heterogeneity, was modeled as a function of the number of segments (n), characterizing spatial resolution of the measurement, using two independent pairs of mutually dependent parameters: the first pair describes v as a power function of n, and the second pair adds a correction for n small. n was varied by joining equal numbers of neighboring segments. Local similarity of the perfusion was characterized by the correlation between the perfusions of neighboring segments. Genesis of the perfusion distribution was modeled by repeated asymmetric subdivision of the perfusion into a volume among two equal subvolumes. These analyses were applied to study the differences between 16 syndrome X patients and 16 age- and sex-matched healthy volunteers using ^{13}N-ammonia parametric PET perfusion data with a spatial resolution of 480 segments. **Results:** The heterogeneity of patients is higher for the whole range of spatial resolutions considered ($2 \leq n \leq 480$; for $n = 480$, $v = 0.22 \pm 0.03$ and 0.18 ± 0.02; $p < 0.005$). This is because the first pair of parameters differs between patients and volunteers ($p < 0.005$), whereas the second pair does not ($p > 0.1$). For both groups of subjects there is a significant positive local correlation for distances up to 30 segments. This correlation is a formal description of the patchy nature of the perfusion distribution. **Conclusion:** When comparing values of v, these should be based on the same value of n. The model makes it possible to calculate v for all values of $n \leq 480$. Mean perfusion together with the two pairs of parameters are necessary and sufficient to describe all aspects of the perfusion distribution. For n small, heterogeneity estimation is less reliable. Patients have a higher heterogeneity because their perfusion distribution is more asymmetrical from the third to the seventh generation of subdivision ($8 \leq n \geq 128$). Therefore, a spatial resolution of $n \geq 128$ is recommended for parametric imaging of perfusion with PET. Patients have only a very slightly more patchy distribution than volunteers. The differences in perfusion between areas with low perfusion and areas with high perfusion is larger in patients.

Key Words: perfusion distribution; left ventricle; fractal dimension; syndrome X

J Nucl Med 1998; 39:1312–1319

Left ventricular myocardial blood perfusion (LVMBP) can be investigated in humans using PET with ^{13}N-ammonia as a tracer (*1–5*). The perfusion distribution is generally characterized by the mean perfusion μ, together with the coefficient of variation v (v = s.d./mean), as a measure of the heterogeneity. Both are important characteristics for studying different groups of patients (*6–10*).

The value of v depends on the number of segments n on which the calculation of v is based. n characterizes the spatial resolution of the measurement. Consequently, measurements with different spatial resolutions (*6,7,11–13*) are not comparable.

Bassingthwaighte et al. (*14–18*), King et al. (*19*) and van Beek et al. (*20,21*) have analyzed the heterogeneity of LVMBP in animals, based on measurements with microspheres and with the tracer iododesmethylimipramine. They used the concept of self-affinity or invariance with respect to scaling (*14,16,17,21*), analyzed the correlation between the perfusions of neighboring segments (*15,21*) and investigated the genesis of the perfusion distribution (*17,19–21*).

These approaches were synthesized and described here. A mathematical model was developed to analyze the influence of the spatial resolution of the measurement on the heterogeneity of ^{13}N-ammonia PET-determined LVMBP. Local similarity of the perfusion was analyzed to clarify the meaning of the model parameters. The genesis of the perfusion distribution was modeled to analyze whether other aspects were overlooked; because μ and v are invariant for permutations of the segments, the description of the distribution is very likely incomplete using only these two characteristics. The minimal number of independent model parameters that is necessary and sufficient to describe the distribution of LVMBP was selected. The method of analysis of LVMBP was tested in patients with syndrome X compared with that in age- and sex-matched healthy volunteers.

Syndrome X denotes the combination of typical angina pectoris and exercised-induced ST-segment depression despite angiographically normal coronary arteries (*22*). The cause(s) and anatomical location are not well known (*23*). Recently, we showed that, in syndrome X patients, LVMBP was more heterogeneous in addition to an increased resting value (*6*).

MATERIALS AND METHODS

Theory

The coefficient of variation of the perfusion v has self-affinity for a limited range of scales (*14,16,17,19*). The relationship between v and the number of segments n into which the myocardium is divided or spatial resolution of the measurement is then:

$$v = v(n) = v_0 \times n^{D-1}, \qquad \text{Eq. 1}$$

where D is the fractal dimension ($D \geq 1$) and v_0 is the extrapolated value of v for $n = 1$. Equation 1 gives a straight line in a double logarithmic plot; however, v is always overestimated for small n. To obtain an equation also valid for small values of n, an exponential function with parameters a_0 and a_1 ($a_0 \geq 0$ and $a_1 \geq 0$) was subtracted from the straight line. This gives an equation with four parameters. In a double logarithmic plot (Fig. 1):

$$lb(v(n)) = lb(v_0) + (D - 1) \times lb(n) - a_0 \times e^{-a_1 \cdot lb(n)}, \qquad \text{Eq. 2}$$

Received Apr. 23, 1997; revision accepted Nov. 21, 1997.

For correspondence or reprints contact: Klaas R. Visser, PhD, Department of Cardiology, University Hospital Groningen, P.O. Box 30.001, NL-9700 RB Groningen, The Netherlands.

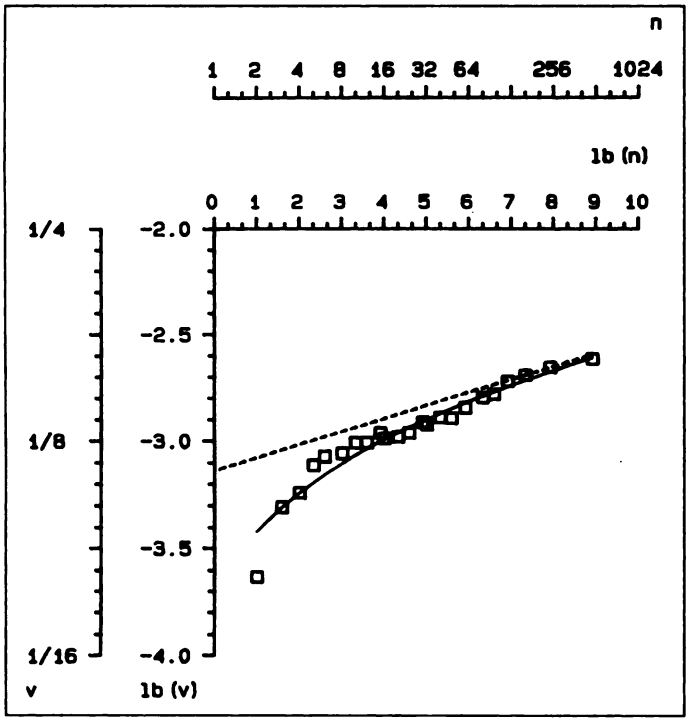

FIGURE 1. Example of estimation of the model parameters. x-axis: binary logarithm of the number of segments n; y-axis: binary logarithm of the coefficient of variation v. The values of v (squares) are calculated from data of one of the volunteers. The solid line is the regression line with Equation 2, $lb(v_0) = -3.14$, D-1 = 0.06, $a_0 = 0.52$, $a_1 = 0.42$ and $v_{cal} = 0.01$ (v_{cal} is a measure for the goodness of fit, Eq. 4). The dotted line is the straight line part of Equation 2 with the same values for the parameters $lb(v_0)$ and D-1.

where lb is the binary logarithm (logarithm to base 2). In a double linear plot:

$$v(n) = v_0 \times n^{D-1} \times e^{-b_0 \times n^{-b_1}}, \qquad \text{Eq. 3}$$

where $b_0 = a_0 \times \ln(2)$ and $b_1 = a_1/\ln(2)$. For large n, the exponential function in Equation 2 approaches 0, leaving a straight line, and the exponential function in Equation 3 approaches 1, leaving a power function (Eq. 1). n was varied by joining equal numbers m of neighboring segments, i.e., n = N/m, where N is the original number of segments ($2 \leq n \leq N$; $1 \leq m \leq N/2$; N = 480).

Local similarity is characterized by the autocorrelation function $\rho(i)$, which is the correlation coefficient of the perfusions of segments and the distance i between the segments. For the unit of distance, the distance between two adjoining segments is taken. In Appendix 1, v as a function of n is transformed into ρ as a function of m, where the distance i is now replaced with distance m = N/n.

The genesis of the perfusion distribution is described by a tree, which is here a process of repeated subdivision of a volume into equal subvolumes, where each subvolume is perfused by a fraction of the flow through the volume. The fractions may be mutually different and different for each generation of subdivision. If the number of subvolumes h is constant for each generation of subdivision, it is possible to derive the relations between v(n) and the fractions. This was worked out in Appendix 2 for arbitrary values of h. The fractions can only be calculated from v(n) for h = 2 (Equation 14A in Appendix 2). Therefore, this model is only used here with h = 2. The i-th generation of subdivisions can then be characterized by one fraction p_i; the other fraction is then $1 - p_i$ (Fig. 2).

PET

With ^{13}N-ammonia PET, LVMBP was quantified using 480 segments. The results were displayed in parametric polar maps (*2*), consisting of 10 rings, each with 48 segments. Each ring represents a slice perpendicular to the basis-apex axis. The instrumentation and measurement procedure were described in detail previously (*2,6*).

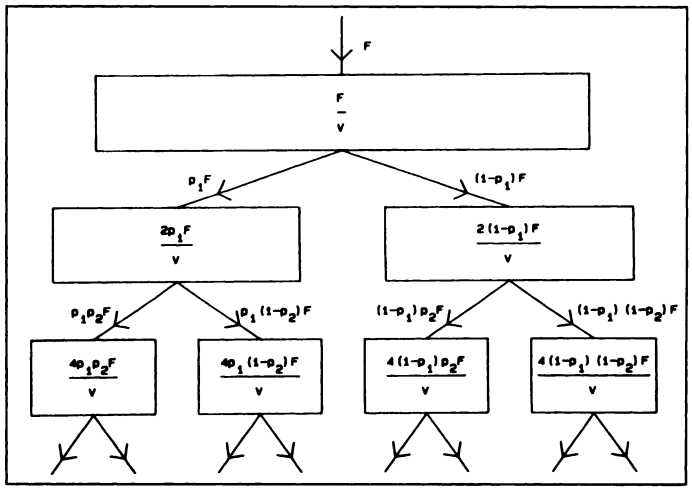

FIGURE 2. Tree dividing into two branches. F is the total flow into the volume V, represented by a rectangle. V is divided into two equal volumes, which each are again divided into two equal volumes and so on. p_1 and $1 - p_1$ are the fractions into which the flow is divided in the first generation of branching, p_2 and $1 - p_2$ are the fractions into which the flow is divided in the second generation of branching and so on. In each rectangle, the perfusion is given next to the lines, indicating the subdivision of the volumes. The values of the flows into the volumes are given.

Subjects

LVMBP was measured in 16 syndrome X patients (9 males) and in 16 age- and sex-matched healthy volunteers. The investigation confirmed to the principles outlined in the Declaration of Helsinki. The study was approved by the ethics committee of the University Hospital Groningen, and each subject gave written informed consent. All participants were nonsmoking, normotensive and nondiabetic. The patients were 30–60 yr (mean ± s.d. = 50 ± 8 yr) and had a normal left ventricle ejection fraction (mean ± s.d. = 0.65 ± 0.04). The volunteers were 25–60 yr of age (mean ± s.d. = 49 ± 8 yr). They were matched for sex and age (within 5 yr) to the patients. This is essentially the same group as that described previously (*6*); however, one pair was replaced by another with a better match, and a second pair was replaced because the patient had additional complaints.

Calculations

The value of v was calculated for all numbers of segments n obtainable by joining an equal number of neighboring segments. For each heart, 23 values of n and v were obtained (n_i = 2, 3,... ,160, 240, 480; i = 1,... ,23). The segments were joined starting with the first segment of the first ring, then the second segment and so on. After 48 segments, the next ring was passed in the opposite direction and so forth. This change of direction each time a ring was completed was done to allow the application of the model for the genesis of the perfusion distribution. The starting segment was always located at a corresponding anatomical position. All segments were treated in the same way.

The four parameters of Equation 2 [$lb(v_0)$, (D-1), a_0 and a_1] were estimated using nonlinear regression analysis. Because the values of lb(v) for large values of n are more accurate than those for small values, we supposed that $\sigma_i \propto 1/\sqrt{n_i}$ where σ_i is the s.d. of the i-th observed value of lb(v), and we used regression analysis with weights $w_i \propto 1/\sigma_i$.

The differences between observed (obs) and estimated (est) values of lb(v) are reported as a coefficient of variation v_{cal}:

$$v_{cal} = \frac{\sqrt{\frac{\sum_{i=1}^{n_p}(w_i \times (lb(v_i)_{obs} - lb(v_i)_{est}))^2}{n_p - n_f}}}{\left|\frac{\sum_{i=1}^{n_p} w_i \times lb(v_i)_{obs}}{n_p}\right|}, \quad \text{Eq. 4}$$

where n_p is the number of data points ($n_p = 23$) and n_f is the number of degrees of freedom of the model ($n_f = 4$). Because $lb(v) < 0$, we have taken the absolute value of its weighted mean. This is the same equation as that used by van Beek et al. (*21*), but was adapted to the use of weights w_i ($w_i \propto \sqrt{n_i}$; the w_i values are normalized so that $\Sigma w_i = n_p$).

The estimated values of the parameters v_0, D-1, a_0 and a_1 were used to obtain estimates of v for all values of n_i ($i = 1, \ldots, 23$) using Equation 3. For $1 \leq m \leq 240$, $\rho(m)$ was calculated directly from the perfusion data, estimated values for $\rho(m)$ were obtained using Equations 7A and 8A (for $m = 1$) in Appendix 1 with the estimated values of v. The required values of v for noninteger values of $n = N/m$ were obtained by interpolation using Equation 3 as a continuous function of n. Because 480 is not a power of 2, the fractions p_i were not calculated directly; estimated values for p_i for the range $1 \leq i \leq 9$ were obtained using Equation 14A of Appendix 2, partly by interpolation and partly by extrapolation, with the estimated values of v and $h = 2$.

Statistics

As a measure of correlation, Spearman's rank correlation coefficient ρ_S was used. ρ_S was also used as a test statistic for independence of the variables. These tests were partly executed one-sided because it was expected that curves with large values of D-1 should have small values of $lb(v_0)$ and the other way around (*16,18,19*). It was also expected that curves with large values of a_1 should have large values of a_0.

The results of patients and volunteers were compared using Wilcoxon's signed-ranks test. These tests were executed one-sided because it was expected that patients had a larger mean perfusion (*6,7,12*) and a larger coefficient of variation than their matched volunteers (*6,7*). The significance of ρ was also tested. Values of test statistics with $p < 0.05$ were considered significant.

RESULTS

Perfusion data are summarized in Table 1, model parameters are summarized in Table 2 and rank correlation coefficients are summarized in Table 3. A summary of the results, based on the mean values of the model parameters, for the coefficient of variation v(n), the autocorrelation function $\rho(m)$ and the fractions p_i is given in Figure 3.

Heterogeneity

The mean μ and the heterogeneity v are two different and independent aspects of the distribution of LVMBP (Table 3). The parameters D-1 and $lb(v_0)$ (Equation 2) are significantly correlated for patients and volunteers; the same holds true for a_0 and a_1 (Equation 2) for patients (Table 3). This is also demonstrated in Figure 4. All points representing $lb(v_0)$ and D-1 clearly belong to one group; the same holds true for the points representing $ln(a_0)$ and a_1. Separate regression lines calculated for patients and volunteers each did not differ significantly. As D-1 and $lb(v_0)$ as well as a_0 and a_1 are not independent quantities (Table 3), we replaced each pair of values by one value, indicated as $\langle v_0,D\rangle$ and $\langle a_0,a_1\rangle$, for the purpose of statistical testing. As we have no knowledge of which quantities should be chosen as independent parameters of the regression lines, the regression lines are not normal (minimizing the sum of the squared vertical distances between data points and line) but are lines minimizing the sum of the squared shortest distances between data points and line. As the test value, the nearest point on the regression line to a data point was chosen. These points were represented by one coordinate, giving their position on the line. $\langle v_0,D\rangle$ and $\langle a_0,a_1\rangle$ or the straight lines and the exponential curves (Fig. 1) represent two different aspects of the heterogeneity; the heterogeneity for n large can be separated from the correction for n small (Table 3).

The estimated values of v for all values of n were also compared. The same result as that for $n = 480$ (Table 1) was obtained (patients have a higher v than volunteers), however only for $n \geq 15$. If the observed values were used, the result remained the same but with a more restricted range: $n \geq 24$.

TABLE 1
Perfusion Data

	Patients (n = 16)		Volunteers (n = 16)	
	Perfusion [ml/(min · 100 g)]	v	Perfusion [ml/(min · 100 g)]	v
Mean	128	0.22	86*	0.18†
s.d.	33	0.03	16	0.02
s.d./mean	0.26	0.14	0.18	0.14
Minimum	89	0.17	64	0.14
Maximum	220	0.26	118	0.22
Median	118	0.22	84	0.18

*$p < 0.0005$ (one-sided).
†$p < 0.005$ (one-sided).
Perfusion = mean perfusion; v = estimated values of the coefficient of variation v for n = 480. The mean and s.d. are given, as well as s.d. as a fraction of the mean, the minimal vlaue, the maximal value and the median. The significances of differences between patients and volunteers are indicated as superscripts at the mean values of the volunteers.

Local Similarity

The autocorrelation function $\rho(m)$ can be described by three (D-1, a_0 and a_1) of the four parameters of Equation 2 (Eqs. 7A and 8A of Appendix 1). However, in Equation 7A, the contribution of D-1 cannot be separated from the contributions of a_0 and a_1 (Appendix 1). Therefore, no conclusions about $\rho(m)$ could be obtained by comparing the parameters. Only for $m = 1$ were the estimated values of $\rho(m)$ significantly higher for patients than for volunteers (Fig. 3, middle). The observed values of ρ showed no significant difference for any value of m; $\rho(m)$ is more a measure of the resemblance between patients and volunteers than of the difference. The significance of $\rho(m)$ for each group of subjects was estimated using the mean values of the model parameters. For both groups there was a significant positive correlation for $m \leq 30$ (Fig. 3, middle).

Genesis of the Perfusion Distribution

In Equation 14A (Appendix 2), the contributions of v_0 and D cannot be separated from the contributions of a_0 and a_1. Therefore, no conclusions about the fractions p_i (Fig. 2) could be obtained by comparing the parameters. The estimated values of p_i for each group of objects were compared for $1 \leq i \leq 9$. The p_i values of the patients were significantly smaller for $3 \leq i \leq 7$ (Fig. 3, right).

TABLE 2
Model Parameters

	Patients (n = 16)					Volunteers (n = 16)				
	$lb(v_0)$	D-1	a_0	a_1	v_{cal}	$lb(v_0)$	D-1	a_0	a_1	v_{cal}
Mean	−2.5	0.04	3.0	0.42	0.035	−3.1*	0.08*	2.3†	0.40†	0.023
s.d.	0.4	0.03	1.5	0.02	0.019	0.4	0.04	1.4	0.02	0.008
s.d./mean	−0.14	0.6	0.5	0.05	0.55	−0.12	0.5	0.6	0.05	0.35
Minimum	−3.2	0.00	0.7	0.38	0.012	−3.7	0.02	0.4	0.36	0.011
Maximum	−1.9	0.09	5.5	0.44	0.082	−2.4	0.16	5.8	0.43	0.045
Median	−2.6	0.04	3.0	0.42	0.031	−3.1	0.08	2.0	0.40	0.023

$lb(v_0)$, D-1, a_0 and a_1 are the parameters of Equation 2. v_{cal} is a measure of the goodness of fit of the model (Eq. 4). Mean value and s.d. are given, as well as s.d. as a fraction of the mean, minimal value, maximal value and median. The significances of differences between patients and volunteers are indicated as superscripts at the mean values of the volunteers. For this test, $lb(v_0)$ and D-1 as well as a_0 and a_1 are taken together, as explained in the text.

DISCUSSION

The Model

Heterogeneity of LVMBP, characterized by the coefficient of variation v, is modeled here by the sum of two functions of the spatial resolution, characterized by the number of segments n (Equation 2 or 3, Fig. 1). The goodness of fit of this model, characterized by v_{cal} (Equation 4), must be judged to be excellent (Table 2); the values of v_{cal} are comparable with or slightly better than those of van Beek et al. (*21*). The two-dimensional parameters, $\langle v_0,D\rangle$ and $\langle a_0,a_1\rangle$, or the straight lines and the exponential curves (Fig. 1) combined with the mean μ are, therefore, necessary to describe the perfusion distribution. If μ is known together with v as a function of n, then the perfusions of all segments can be calculated using a tree with the number of subvolumes per generation of subdivision h = 2 (Appendix 2). Consequently, $\langle v_0,D\rangle$ and $\langle a_0,a_1\rangle$, together with μ, are also sufficient to describe the perfusion distribution for h = 2. For other values of h, the distribution always lies between two fully specified distributions based on h = 2, because v can be considered a continuous function of n. Therefore, $\langle v_0,D\rangle$ and $\langle a_0,a_1\rangle$ together with μ are necessary as well as sufficient to describe the distribution of the LVMBP.

TABLE 3
Spearman's Rank Correlation Coefficients

	Patients (n = 16)						Volunteers (n = 16)					
	Perfusion	v	v_0	D	a_0	$\langle v_0, D\rangle$	Perfusion	v	v_0	D	a_0	$\langle v_0, D\rangle$
v	0.2						0.4					
v_0	0.3	0.7*					−0.3	0.3				
D	−0.3	−0.3	−0.8*				0.4	0.2	−0.8*			
a_0	−0.07	−0.1	0.4	−0.5*			−0.04	−0.2	0.2	−0.3		
a_1	0.06	0.03	0.4	−0.7*	0.5*		−0.3	−0.1	0.7*	−0.8*	0.4	
$\langle v_0, D\rangle$	−0.3	−0.7*					0.3	−0.3				
$\langle a_0, a_1\rangle$	−0.07	−0.1				−0.4	−0.04	−0.2				−0.2

Perfusion = mean perfusion; v = estimated value of v for b = 480; v_0, D-1, a_0 and a_1 are the model parameters of Equation 2. As ρ_s is based on ranks, the values of ρ_s for $\ln(v_0)$ are equal to those of v_0, and the same holds true for D-1 and D and for $\ln(a_0)$ and a_0; therefore these values are not shown. Because v_0 and D-1 as well as a_0 and a_1 are not independent, they are treated as one quantity as described in the text. These quantities are indicated as $\langle v_0, D\rangle$ and $\langle a_0, a_1\rangle$.

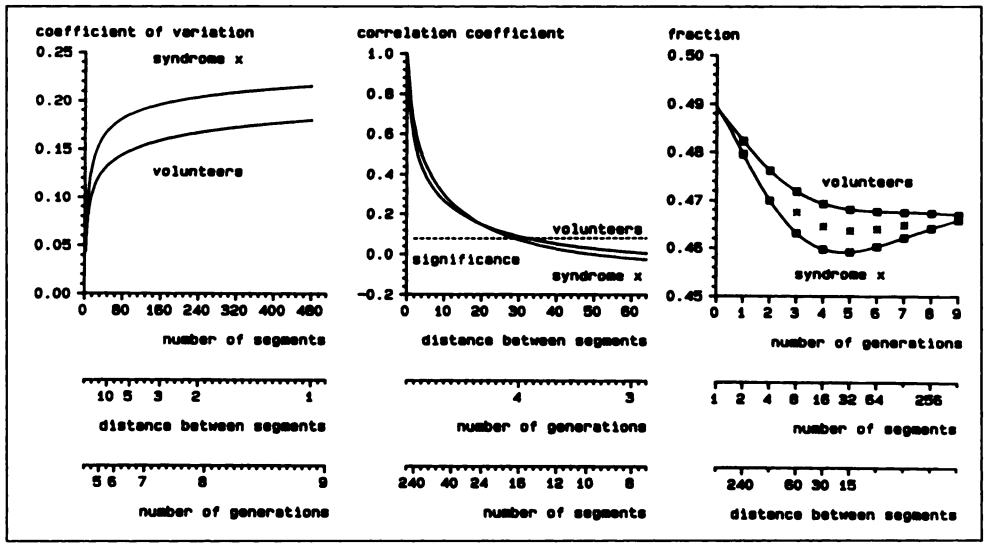

FIGURE 3. Summary of the results. Above the dotted line, the correlation is significantly different from zero (middle). Significantly different fractions are indicated with an asterisk between the data points (right). The functions shown are all discrete functions of the independent variables. For the sake of simplicity, they are presented here as continuous functions, only the estimated values of the fractions are also presented. The variables of all three horizontal axes can be transformed into each other, as shown by two extra axes in each panel.

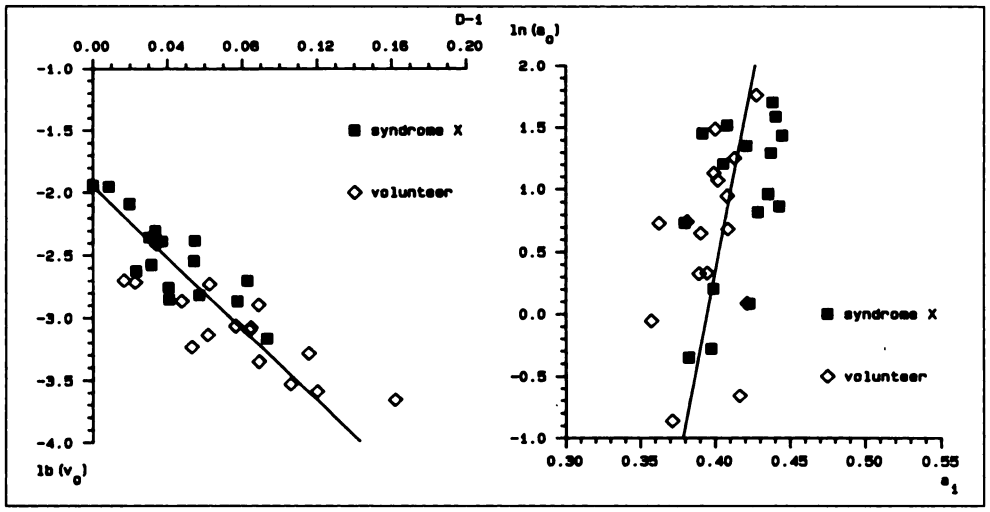

FIGURE 4. Estimated values D-1 as function of $lb(v_0)$ and of $ln(a_0)$ as a function of a_1. The points represent the $lb(v_0)$ and D-1 values of each subject (left) and the values of $ln(a_0)$ and a_1 (right) together with the regression lines $lb(v_0) = -1.95–14.35 \times (D-1)$ ($n = 16$, $r = 0.85$) and $ln(a_0) = -24.27 + 61.48 \times a_1$ ($n = 16$, $r = 0.48$). The regression lines minimize the sum of the squared shortest distances between data points and line.

As one of the functions (the straight line), describing v as a function of n (Equation 2) differs between patients and volunteers and the other (the exponential function) does not (Table 2), the sum of these two functions also differs. This implies that the heterogeneity of syndrome X patients is higher than that of healthy volunteers for the whole range of spatial resolutions ($2 \leq n \leq 480$; Fig. 3, left). This conclusion may not have been reached when using a lower maximal resolution ($N < 480$) because v is different for n large, while the correction for n small is the same. This is corroborated by using less advanced data reduction schemes; the conclusion holds for $n \geq 15$ when using estimated values of v and for $n \geq 24$ when using observed values of v. The difference between the mean distributions increases from $i \geq 3$ or $n \geq 8$ up to $i = 7$ or $n = 128$ (Fig. 3, right), with i being the number of the generation of subdivision. Thus an optimal resolution would be $n \geq 128$.

The values of D (Table 1) are smaller than those reported by Bassingthwaighte et al. (*14*), who found a mean value of approximately 1.2 with different measurement techniques (deposition of microspheres and tracers) and in various species (baboons, sheep and rabbits). This can be expected because we considered self-affinity as an approximation for large n instead of description for all values of n, whereas there may also be a species dependency of D.

The perfusion distribution is treated as a one-dimensional problem. This gives a fractal dimension between 1 and 2, in agreement with the fact that the value of D lies between the Euclidean dimension and one plus this dimension (*24*). However, we use, in fact, a two-dimensional projection of the left ventricle, so $2 \leq D \leq 3$. van Beek (*20*) has shown that the fractal dimension for this situation is exactly 1 higher than the D obtained by using Equation 2.

We have reduced a two-dimensional to a one-dimensional problem by combining the segments in a special way. As already remarked by Bassingthwaighte et al. (*14*), the segments can be joined in many different ways. As there are no other criteria for joining the segments than doing it always in the same way so as to make the results mutual comparable and doing it so as to make the model for the genesis of the distribution applicable, we have chosen the way that is indicated by the geometry of the measurement; it is the obvious way to link the concept of spatial resolution to the measurement set-up.

Heterogeneity is considered here as a function of the spatial resolution of the measurement. This is an instrumental characteristic. Different causes of heterogeneity can be distinguished: spatial, temporal and methodological (*16,25*). These causes have been separated by performing succeeding and simultaneous microsphere measurements (*16,25*), but this is not feasible for PET measurements. However, by employing nonparametric statistics, our conclusions are not influenced by methodological variations.

For patients and volunteers the autocorrelation function $\rho(m)$ is significantly positive for $m \leq 30$ (Fig. 3, middle). This means that segments with high perfusion tend to have neighbors with high perfusion, and segments with low perfusion tend to have neighbors with low perfusion. Therefore, this positive correlation is a formal description of the patchy nature of the perfusion distribution: the smaller the value of ρ or the larger the value of D (in case of self-affinity or m small), the less patchy the nature of the distribution. Syndrome X patients have only a very slightly more patchy distribution than healthy volunteers (only for $m = 1$ the values of ρ differ). If the patchy character of the distribution is not quantified or compared with that in healthy subjects, one may easily attribute this character as being unique to syndrome X patients (*26,27*). The striking distinction is that the differences in perfusion between areas with a low perfusion and areas with a high perfusion is larger in patients than in volunteers (higher value of v_0). These differences are more pronounced for higher values of n. The positive correlation over short distances has previously been reported in (healthy) experimental animals: dogs (*28*) and baboons (*15*).

For self-affinity, van Beek et al. (*21*) have shown that:

$$\rho(1) = 2^{3-2D} - 1 \quad \text{for} \quad 1 \leq D \leq 2, \qquad \text{Eq. 5}$$

where $\rho(1)$ is the correlation coefficient for perfusions between nearest neighboring segments and D is the fractal dimension. Bassingthwaighte and Beyer (*15*) have extended this to nonadjacent neighbors. This was further extended (in Appendix 1) for the more general case of v a function of n, and ρ a function of m ($m = N/n$). Equation 5 is Equation 8A with Equation 1 inserted for v(n). The relation of Bassingthwaighte and Beyer is Equation 7A with Equation 1 substituted for v(n).

Self-affinity is treated here as a limiting situation for n large, thereby adding two parameters (a_0 and a_1). Bassingthwaighte et al. (*17,18*) and van Beek et al. (*20,21*) used a tree with $h = 2$ to describe the origination of the heterogeneity. The calculation procedure is the same (i.e., varying n by joining an equal number of neighboring segments), but the interpretation of the results is different. We extended their approach for arbitrary values of h (Appendix 2). They made various assumptions for the values of the fractions (*18,20,21*). If a relation between v and n is available for the whole range of spatial resolutions ($2 \leq$

$n \leq N$), then it is not necessary to make any assumption for the fractions p_i to apply this model with $h = 2$ (Appendix 2) (*21*). We used this model purely as a description of the genesis of the distribution, not linking it in any way to an actual vascular tree (*18,20,21*) because we consider this too speculative.

We have extended the previous reported approaches to model LVMBP heterogeneity (*14–21*) and applied them to human PET data:

1. By using all possible integer values for n, because theory does not dictate only powers of 2 as previously used (hence the use of binary logarithms);
2. By including in our model values of n where the self-affinity model does not hold, through introducing an additional exponential function for small values of n;
3. By taking into account the fact that values of lb(v) based on large values of n are more accurate than those based on smaller values of n;
4. By showing the mutual dependency of D-1 and $lb(v_0)$ and of a_0 and a_1 (Fig. 4 and Table 3); the mutual dependency of D-1 and $lb(v_0)$ has previously been shown for LVMBP of baboons, sheep and rabbits based on microspheres data (*16,18,19*); and
5. By establishing the relations between the different approaches (Appendices 1 and 2 and Fig. 3).

Patients Compared with Volunteers

The increased mean value and increased heterogeneity of the LVMBP in syndrome X patients have been described previously (*6,7,12*). Rosen et al. (*13*) and Geltman et al. (*12*) found no difference in mean perfusion and heterogeneity between patients and healthy controls using $H_2{}^{15}O$ combined with $C^{15}O$ as tracers. Neither performed a paired test, but instead tested the differences between the groups, so that individual differences might disappear because of the large spread of the data. They tested two-sided instead of one-sided, which may lead to a false conclusion if the mean difference between the groups is small. Rosen et al. (*13*) used a lower spatial resolution ($n = 60$), whereas Geltman et al. (*12*) used three or four segments. The patients of Geltman et al. (*12*) had a marked different range of ages compared to their control group (40–73 yr versus 20–35 yr). Camici et al. (*11*) did not compare patients with healthy subjects. The large spread in the individual data of the mean perfusion is generally noticed, but the fact that the mean perfusion is an independent quantity is not (*7,11–13*).

CONCLUSION

The coefficient of variation v of LVMBP is a monotonously nondecreasing function of the number of segments n or spatial resolution of the measurement (Appendix 2). When comparing values of v, these should be based on the same value of n. The model makes this possible for all n smaller than the total number of segments used ($N = 480$). The independent two-dimensional parameters $\langle v_0, D\rangle$ and $\langle a_0, a_1\rangle$ (Fig. 1 and Equaiton 2) represent two different aspects of the heterogeneity: the heterogeneity for n large can be separated from the correction for n small (Table 3). These parameters combined with the mean μ are necessary and sufficient to describe the distribution of the LVMBP. The heterogeneity of syndrome X patients is higher than that of healthy volunteers for the whole range of spatial resolutions considered ($2 \leq n \leq 480$; Fig. 3, left).

The relation between v and the local similarity, characterized by the autocorrelation function $\rho(m)$ with m the distance between segments, was established (Appendix 1). ρ depends only on the shape of v, not on its magnitude. Only $\rho(1)$ is significantly higher for patients compared to volunteers. Both patients and volunteers had a significant positive correlation for $m \leq 30$. This positive correlation is a formal description of the patchy nature of the perfusion distribution.

The generation of heterogeneity was modeled by repeated asymmetric subdivision of the perfusion into a volume among two equal subvolumes. The perfusion distribution of the patients was significantly more asymmetrical from the third through the seventh generation of subdivision. Therefore, an optimal resolution would be $n \geq 128$.

The high similarity between the distributions of patients and healthy volunteers (Fig. 4) indicates that the cause of the difference in the distributions is either homogeneously distributed for the spatial resolutions considered ($2 \leq n \leq 480$) or has a location beyond the maximal resolution ($n > 480$). The character of the difference in perfusion distribution between patients and volunteers (i.e., the differences in perfusion between areas with a low perfusion and areas with a high perfusion is larger in patients compared to volunteers) is in favor of the latter hypothesis. This latter hypothesis is in also agreement with the concept that increased resistance of the prearteriolar coronary vessels is the fundamental abnormality in syndrome X patients (*27*).

ACKNOWLEDGEMENTS

We thank Ir. L.E. Weijs for his critical reading of the manuscript and his careful checking of the mathematics.

APPENDIX 1:

Autocorrelation Function

We consider N volumes V_k ($k = 1,\ldots, N$), ordered in such a way that V_k and V_{k+1} always adjoin each other. We form groups of m neighboring volumes: $V_{k+1}, V_{k+2},\ldots, V_{k+m}$, with perfusions: $q_{k+1}, q_{k+2},\ldots, q_{k+m}$. For the variance σ^2 applies (*29*):

$$\sigma^2\left(\sum_{i=1}^{m} q_{k+i}\right) = \sum_{i=1}^{m} \sigma^2(q_{k+i}) + 2\sum_{i=1}^{m-1}\sum_{j=i+1}^{m} \mathrm{cov}(q_{k+i}, q_{k+j})$$

$$\sigma^2(N/m) = m \times \sigma^2(N) + 2\sum_{i=1}^{m-1}\sum_{j=i+1}^{m} \mathrm{cov}(q_{k+i}, q_{k+j}), \qquad \text{Eq. 1A}$$

where $\mathrm{cov}(q_{k+i}, q_{k+j})$ is the covariance of q_{k+i} and q_{k+j}. We assume that σ depends only on the number of elements. The correlation coefficient $\rho(i,j)$ between two perfusions q_i and q_j is (*29*):

$$\rho(i,j) = \frac{\mathrm{cov}(i,j)}{\sqrt{\sigma^2(q_i)\sigma^2(q_j)}} = \frac{\mathrm{cov}(i,j)}{\sigma^2(N)}, \qquad \text{Eq. 2A}$$

where $\mathrm{cov}(q_i, q_j)$ is notated as $\mathrm{cov}(i,j)$. Equation 1A can be rewritten as:

$$2 \times \sum_{i=1}^{m-1}\sum_{j=i+1}^{m} \rho(k+i, k+j) = \frac{\sigma^2(N/m)}{\sigma^2(N)} - m. \qquad \text{Eq. 3A}$$

Dividing each variance in Equation 3a by the square of its mean gives:

$$2 \times \sum_{i=1}^{m-1}\sum_{j=i+1}^{m} \rho(k+i, k+j) = m^2 \times \frac{v^2(N/m)}{v^2(N)} - m, \qquad \text{Eq. 4A}$$

where v is the coefficient of variation.

We consider ρ as a function of the distance between the volumes. For the unit of the distance we take the distance between two

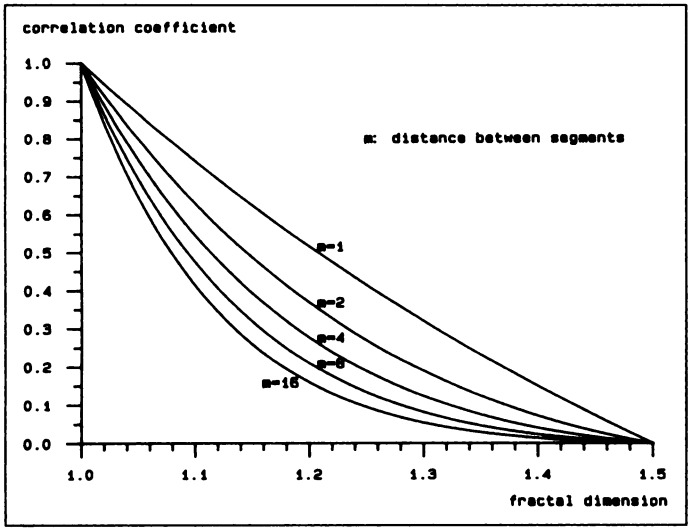

FIGURE 5. The correlation coefficient $\rho(m)$ as a function of the fractal dimension D for different values of the distance between the segments m. The equation of the plotted lines is Equation 7A with Equation 3 for v(n). This gives an equation that is applicable in case of self-affinity.

adjoining volumes. As the volumes are numbered in succession, for every value of k applies:

$$\rho(k, k + i) = \rho(i). \qquad \text{Eq. 5A}$$

The double sum in Equation 4A has now many equal terms, leading to:

$$2 \times \sum_{i=1}^{m-1} (m - i) \times \rho(i) = m^2 \times \frac{v^2(N/m)}{v^2(N)} - m. \qquad \text{Eq. 6A}$$

If we replace m with m + 1 and with m − 1 in Equation 6A, we get:

$$\rho(m) = \frac{(m+1)^2 \times v^2\left(\frac{N}{m+1}\right) - 2 \times m^2 \times v^2\left(\frac{N}{m}\right) + (m-1)^2 \times v^2\left(\frac{N}{m-1}\right)}{2 \times v^2(N)}.$$

Eq. 7A

This equation is valid for integer values of $N \geq 6$ and $m \geq 2$. $\rho(o) \equiv 1$. For m = 2 and $N \geq 4$, Equation 6A gives:

$$\rho(1) = 2 \times \frac{v^2\left(\frac{N}{2}\right)}{v^2(N)} - 1. \qquad \text{Eq. 8A}$$

When v is known as a function of the number of segments n = N/m, then ρ, as a function of the distance between segments m, can be calculated from it, but not the other way around; ρ depends only on the shape of v(n), not on its magnitude, i.e., not on v_0 (Eq. 7A).

Combining Equation 7A and Equation 1 gives an equation with only D and m as parameters, which holds for the case of self-affinity, illustrated in Figure 5. In this case, ρ is a monotonously decreasing function of D (with m constant) and also a monotonously decreasing function of m (with D constant). If D = 1.5, then $\rho = 0$ for all values of m, indicating a random distribution. In the case of self-affinity, the value of ρ is independent of the actual dimensions of the segments or the total number of segments N. This illustrates self-affinity or invariance with respect to scaling.

If we define $f(m) = m^2 \times v^2(N/m)$, then, by approximating f(m + 1) and f(m − 1) by a Taylor series, $\rho(m)$ can be written as a series of even derivatives of f(m) with respect to m: $\rho(m) \approx (f^{ii}(m) + f^{v}(m)/12 + \ldots)/(2 \times f(1))$. If we use Equation 3 for v(N/m), we see that $\rho(m)$ can be written as the product of an exponential function with exponent: $-b_0 \times (N/m)^{-b_1}$ and a multinomial in m. The exponential function approaches 0 for large values of m, meaning that there is no correlation for large distances. The multinomial contains mixed terms with D-1, a_0 and a_1. Thus, in Equation 7A the contribution of D-1 cannot be separated from the contributions of a_0 and a_1.

APPENDIX 2:

Genesis of the Perfusion Distribution

We consider a volume V, perfused with a flow F. V is divided into h equal subvolumes with volumes V/h ($h \geq 2$). The first subvolume is perfused with a fraction p_{11} of F, the second subvolume with a fraction p_{12} of F and so on. This subdivision is repeated k times, and each i-th generation of subdivision is characterized by its own fractions p_{ij} (j = 1 ... h):

$$0 \leq p_{ij} \leq 1 \quad \text{and} \quad \sum_{j=1}^{h} p_{ij} = 1 \quad \text{for} \quad i = 1, 2, \ldots, k.$$

Eq. 9A

The h^k perfusions of the different volumes are given by the terms of the product:

$$\frac{h^k \times F}{V} \times \prod_{i=1}^{k} \left(\sum_{j=1}^{h} p_{ij} \right) = \sum_{l=1}^{h^k} q_l(k, h). \qquad \text{Eq. 10A}$$

This representation could be called a tree. If the terms of the product of Equation 10A are always written down in the same sequence, it is possible to attach a number l to each term (l = 1, 2, 3,. . ., h^k) unambiguously; $q_l(k,h)$ is then the l-th perfusion of a volume of the k-th generation of a tree dividing into h branches. The probability (Pr) for the occurrence of a value of q is: $Pr(q_l(k,h)) = 1/h^k$. The mean μ of the perfusions is always: $\mu = F/V$. Realizing that (analog to Eq. 10A):

$$\sum_{l=1}^{h^k} q_l^2(k, h) = \left(\frac{h^k \times F}{V} \right)^2 \times \prod_{i=1}^{k} \left(\sum_{j=1}^{h} (p_{ij}^2) \right), \qquad \text{Eq. 11A}$$

we get for the variance $\sigma^2(n)$ of the perfusions, where n is the number of endbranches ($n = h^k$):

$$\sigma^2(n) = \sigma^2(h^k) = E((q_l(k, h) - \mu)^2) = E(q_l(k, h)^2) - E^2(q_l(k, h))$$

$$= \sum_{l=1}^{h^k} q_l^2(k, h) \times Pr(q_l(k, h)) - \mu^2 = \left(\frac{h^k \times F}{V} \right)^2 \times \prod_{i=1}^{k} \left(\sum_{j=1}^{h} p_{ij}^2 \right)$$

$$\times \frac{1}{h^k} - \mu^2 = \mu^2 \times \left(h^k \times \prod_{i=1}^{k} \left(\sum_{j=1}^{h} p_{ij}^2 \right) - 1 \right), \qquad \text{Eq. 12A}$$

where E is the expectation. The coefficient of variation v is:

$$v(n) = v(h^k) = \frac{\sigma(h^k)}{\mu} = \sqrt{\prod_{i=1}^{k} h \times \left(\sum_{j=1}^{h} p_{ij}^2 \right) - 1}, \qquad \text{Eq. 13A}$$

and reversed:

$$h \times \sum_{j=1}^{h} p_{kj}^2 = \frac{v^2(h^k) + 1}{v^2(h^{k-1}) + 1} = \frac{v^2(n) + 1}{v^2\left(\frac{n}{h}\right) + 1} \approx 1 + v^2(n) - v^2\left(\frac{n}{h}\right).$$

Eq. 14A

The approximation ($\approx$) holds good for $v^4(n) \ll 1$. Equation 9A gives:

$$1 \leq h \sum_{j=1}^{h} p_{ij}^2 \leq h. \qquad \text{Eq. 15A}$$

The lower bound in Equation 15A represents the case of symmetric subdivision ($p_{i1} = p_{i2} = \ldots = p_{ih} = 1/h$); the upper bound represents the case of maximal asymmetric subdivision ($p_{i1} = p_{i2} = p_{i3} = \ldots = p_{ih-1} = 0$, $p_{ih} = 1$). The more asymmetrical the subdivision is, the higher the value of v becomes. As long as the subdivision is asymmetrical, v increases as n increases; if the subdivision becomes symmetrical v stays constant. Therefore, v is a monotonously nondecreasing function of n (Eqs. 13a and 15a).

If the fractions p_{ij} are known, it is always possible to calculate the coefficient of variation v directly from the p_{ij} values (Equation 13A). However, if v is known as a function of n, the p_{ij} values can only be calculated for $h = 2$; the fractions can then be simplified to p_i and $1\text{-}p_i$ (Fig. 2). Equation 10A gives the distribution of the perfusion. When $h = 2$, this distribution could be called (analogous to the log-normal distribution) log-binomial distribution of Poisson (*30*), with the special property that the number of parameters is generally less then k because the p_i values are mutually related.

Combining Equations 14A and 15A with Equation 1, we get:

$$1 \leq \frac{v_0^2 \times n^{2D-2} + 1}{v_0^2 \times \left(\frac{n}{h}\right)^{2D-2} + 1} \leq h. \qquad \text{Eq. 16A}$$

The lower bound is met for $D \geq 1$. The upper bound is only met for all values of n for $D \leq 1.5$. So, $1 \leq D \leq 1.5$; this is also valid for more general versions of this model: h is not the same for each generation and/or the dividing is not constant in a generation.

REFERENCES

1. Bellina CR, Parodi O, Camici PG, et al. Simultaneous in vitro and in vivo validation of nitrogen-13-ammonia for assessment of regional myocardial blood flow. *J Nucl Med* 1990;31:1335–1343.
2. Blanksma PK, Willemsen ATM, Meeder JG, et al. Quantitative myocardial mapping of perfusion and metabolism using parametric polar map displays in cardiac PET. *J Nucl Med* 1995;36:153–158.
3. Schelbert HR, Phelps ME, Huang SC, et al. Nitrogen-13 ammonia as an indicator of myocardial blood flow. *Circulation* 1981;63:1259–1272.
4. Shah A, Schelbert HR, Schwaiger M, et al. Measurement of regional blood flow with N-13 ammonia and positron emission tomography in intact dogs. *J Am Cardiol* 1985;5:92–100.
5. Wisenberg G, Schelbert HR, Hoffman EJ, et al. In vivo quantification of regional myocardial blood flow by positron emission tomography. *Circulation* 1981;63:1248–1258.
6. Meeder JG, Blanksma PK, Crijns HJGM, et al. Mechanisms of angina pectoris in syndrome X assessed by myocardial perfusion dynamics and heart rate variability. *Eur Heart J* 1995;16:1571–1577.
7. Galassi AR, Crea F, Araujo LI, et al. Comparison of regional myocardial blood flow in syndrome X and one-vessel coronary artery disease. *Am J Cardiol* 1993;72:134–139.
8. Hautvast RWM, Blanksma PK, DeJongste MJL, et al. Effect of spinal cord stimulation on myocardial blood flow assessed by positron emission tomography in patients with refractory angina pectoris. *Am J Cardiol* 1996;77:462–467.
9. Meeder JG, Blanksma PK, van der Wall EE, et al. Long-term cigarette smoking is associated with increased myocardial perfusion heterogeneity assessed by positron emission tomography. *Eur J Nucl Med* 1996;23:1442–1447.
10. Posma JL, Blanksma PK, van der Wall EE, Vaalburg W, Crijns HJGM, Lie KI. Effects of permanent dual-chamber pacing on myocardial perfusion in symptomatic hypertrophic cardiomyopathy. *Heart* 1996;76:358–362.
11. Camici PG, Gistri R, Lorenzoni R, et al. Coronary reserve and exercise ECG in patients with chest pain and normal coronary angiograms. *Circulation* 1992;86:179–186.
12. Geltman EM, Henes G, Senneff MJ, Sobel BE, Bergmann SR. Increased myocardial perfusion at rest and diminished perfusion reserve in patients with angina and angiographically normal coronary arteries. *J Am Coll Cardiol* 1990;16:586–595.
13. Rosen SD, Uren NG, Kaski J-C, Tousoulis D, Davies GJ, Camici PG. Coronary vasodilator reserve, pain perception, and sex in patients with syndrome X. *Circulation* 1994;90:50–60.
14. Bassingthwaighte JB. Physiological heterogeneity: fractals link determinism and randomness in structures and functions. *NIPS* 1988;3:5–10.
15. Bassingthwaighte JB, Beyer RP. Fractal correlation in heterogenous systems. *Physica D* 1991;53:71–84.
16. Bassingthwaighte JB, King RB, Roger SA. Fractal nature of regional myocardial blood flow heterogeneity. *Circ Res* 1989;65:578–590.
17. Bassingthwaighte JB, van Beek JHGM. Lightning and the heart: fractal behavior in cardiac function. *Proc IEEE* 1988;76:693–699.
18. Bassingthwaighte JB, van Beek JHGM, King RB. Fractal branchings: the basis of myocardial flow heterogeneities? *Ann NY Acad Sci* 1990;591:392–401.
19. King RG, Weissman LJ, Bassingthwaighte JB. Fractal description for spatial statistics *Ann Biomed Eng* 1990;18:111–121.
20. van Beek JHGM. Fractal model of heterogeneity in organ blood flow. In: Egginton S, Ross HF, eds. *Oxygen transport in biological systems*. Cambridge: Cambridge University Press; 1992:135–163.
21. van Beek JHGM, Roger SA, Bassingthwaighte JB. Regional myocardial flow heterogeneity explained with fractal networks. *Am J Physiol* 1989;257:H1670–H1680.
22. Kemp HG. Left ventricular function in patients with the anginal syndrome and coronary arteriograms. *Am J Cardiol* 1973;32:375–376.
23. Cannon III RO, Camici PG, Epstein SE. Pathophysiological dilemma of syndrome X. *Circulation* 1992;85:883–891.
24. Voss RF. Fractals in nature: from characterization to simulation. In: Peitgen H-O, Saupe D, eds. *The science of fractal images*. New York: Springer; 1988:21–70.
25. King RB, Bassinghwaighte JB, Hales JRS, Rowell LB. Stability of heterogeneity of myocardial flow in normal awake baboons. *Circ Res* 1985;57:285–295.
26. Cianflone D, Lanza GA, Maseri A. Microvascular angina in patients with normal coronary arteries and with other ischemic syndromes. *Eur Heart J* 1995;16:96–103.
27. Maseri A, Crea F, Kaski JC, Crake T. Mechanism of angina pectoris in syndrome X. *J Am Coll Cardiol* 1991;17:499–506.
28. Austin RE Jr, Aldea GS, Coggins DL, Flynn AE, Hoffman JIE. Profound spatial heterogeneity of coronary reserve. Discordance between patterns of resting and maximal myocardial blood flow. *Circ Res* 1990;67:319–331.
29. Parzen E. *Modern probability theory and its applications*. New York: John Wiley and Sons; 1992.
30. Johnson NL, Kotz S, Kemp AW. *Univariate discrete distributions*, 2nd ed. New York: John Wiley and Sons; 1992.